

Decoding of Atmospheric Pressure Plasma Emission Signals for Process Control

Victor J Law¹, F T O'Neill², D P Dowling², J L Walsh³, F Iza³, N B Janson⁴, and M G Kong³

¹Dublin City University, National Centre for Plasma Science and Technology, Collins Avenue, Glasnevin, Dublin 9, Dublin, Ireland.

(e-mail: vic.law@dcu.ie)

²School of Mechanical and Materials Engineering, University College Dublin, Belfield, Dublin 4, Ireland.

³Department of Electronic and Electrical engineering, Loughborough University, Leicestershire LE11 3TU UK.

⁴School of Mathematics, Loughborough University, Leicestershire LE11 3TU UK.

Abstract: Three-dimensional phase-space representation and 3-dimensional surface imaging using single scalar time series data obtained from two very different atmospheric pressure plasma systems is presented. The process of delay embedding, Savitzky-Golay digital filtering and deconvolution of frequency-domain data is described.

Keywords: Plasma, Electrical measurement, Electro-acoustic, Overtones, LabVIEW.

1 Introduction

Low-temperature, non-thermal atmospheric pressure plasma jets (APPJ) are being developed for surface treatment of biomedical devices, sterilisation, and therapeutic techniques, such as wound sterilisation and cancer treatment [1]. In addition to these medical applications, APPJ are now routinely employed in the automotive (car head lamps) and aerospace (fuselage and wing components) industry for surface activation of polymer prior to bonding [2]. This paper describes some of the emerging plasma electrical and electro-acoustic metrology that is being developed for the diagnostics and control of APPJ systems. In particular the requirement for extraction of information that describes the tempo-spatial heterogeneous processes. The methodology to obtain this information is currently in its infancy when compared to low pressure plasma metrology [3]. In this paper the multivariate analysis tools for the 3-dimensional phase-space representation from a single scalar time series, either of a single observable in the time-domain, or temporal-spatial deconvolutions of a single observable in the frequency-domain are given. The use of these tools to obtain measurements on two APP jet systems is presented: a hand-held plasma jet [4]; and an industrial scale computer numerical controlled PlasmaTreat OpenAir™ APPJ system [5 and 6]. By comparing the diagnostic information obtained using these two APPJ systems the robustness of the diagnostic techniques for both



laboratory and industrial scale APPJ are demonstrated.

2 3-D representation of a signal observation: Current

Cold APPJ pens (some times called pencils or needles) are increasingly used in many processing applications due to a distinct combination of their inherent plasma stability with excellent reaction chemistry that is often enhanced downstream. The term *cold* used here refers to temperatures of less than 50°C at the point of contact and so enables the treatment of temperature sensitive living tissue and organic polymers. An example of the helium APPJ pen examined in this study, which is driven at a drive frequency of 18 kHz, is shown in figure 3.1 and discussed in detail in references [1 and 4].

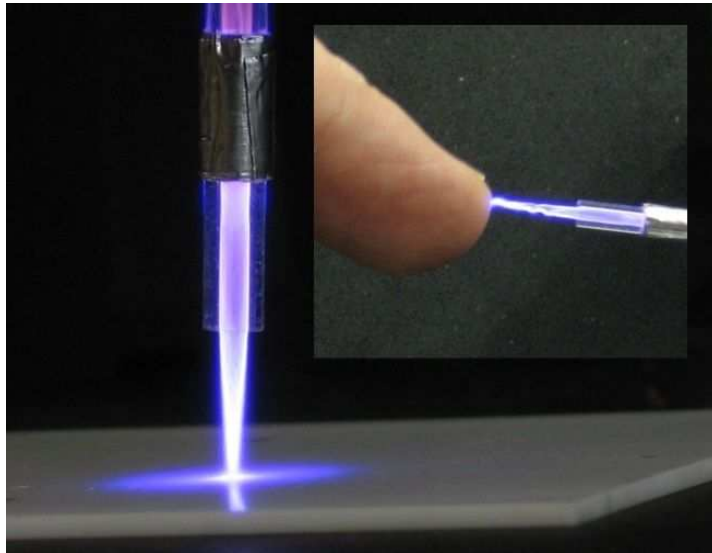


Figure 2.1: Image of a cold AAPJ pen and interaction with human figure.

This section of the paper describes one of the emerging metrology techniques that can characterise the APPJ pen's three modes of operation (chaotic, bullet and continuous). However, when there is access to only one single observable, namely, the current at the driving electrode $I(t)$, defining these modes becomes a challenge. Figure 2.2 details the current waveform for each of the three modes of operation. A common feature of all three modes is that their current waveform has one distinct peak every positive half cycle of the applied voltage and one current peak every negative half cycles, but later this is not always the case. The chaotic mode is observed immediately after breakdown, and an increase in the input power eventually leads to the bullet mode and then to the continuous mode. As the mode changes to bullet and then on to continuous, the current peaks become stronger and regular and finally adding an additional current peak per voltage cycle in the continuous

mode.

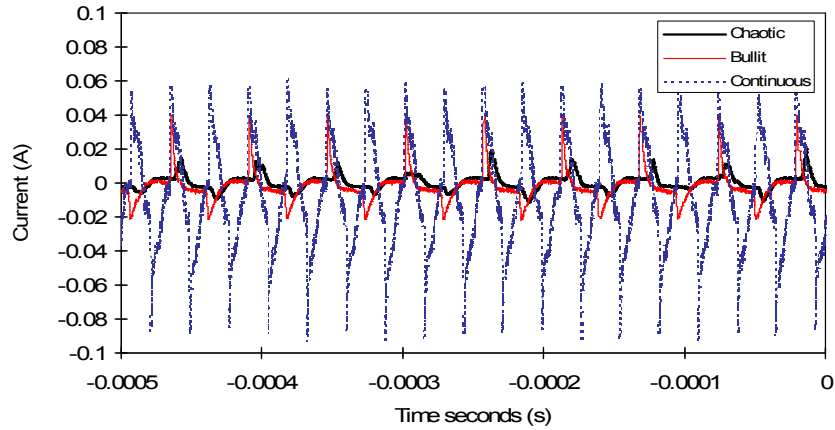


Figure 2.2: APPJ pen current waveforms in the chaotic, bullet and continuous modes.

In order to introduce a phase-space representation of the APPJ current waveform the technique of embedding is used [7]. In particular, we use the delay embedding within which the state vector at time t in the 3-dimensional phase space is reconstructed as a vector whose coordinates are the values of the single observable taken at time moments separated by a certain delay τ , namely, $(I(t), I(t + \tau), I(t + 2\tau), \dots, I(t + (m - 1)\tau))$. The number m is the embedding dimension and depends on the dimension of the attractor in the original dynamical system. For visualization purposes, here we choose $m = 3$. The time delay τ can be chosen by a variety of methods, but one of the most popular approaches is to calculate the mutual information from the variables $I(t)$ and $I(t + \tau)$ as a function of τ , and to choose its first minimum [8]. The value of τ obtained by this method was close to $4\mu\text{s}$ for all datasets and was chosen for the phase-space reconstruction in this study.

Figures 2.3(*chaotic*), (*bullet*) and (*continuous*) shows 3-dimensional phase space reconstructions for the APPJ pen operating in the chaotic, bullet and continuous modes, respectively. For each mode, the phase trajectory is shown during several hundred excitation cycles. Whereas figures 2.3(*bullet*) and (*continuous*) show limit cycles (i.e. periodic attractors), figure 2.3(*chaotic*) shows a set that does not look similar to a limit cycle, nor to a low-dimensional torus representing a quasi periodic (i.e. non-chaotic) behaviour. We therefore suggest that this is a projection of a chaotic Attractor into a three-dimensional space.

An alternative to the 3-dimensional phase-space reconstruction of the current waveform is to cut the block of sequentially sampled data points in to n -frames, with each frame length equal to one complete drive frequency period, T , (where $T = 1/f$, followed by alignment of each frame, to a common zero-crossing-point, within the block of data. The data displayed in figure 2.2 is used for this time-domain reconstruction and has been performed in a LabVIEW program [9] where the recorded length was found to be 555 points per period of the 18 kHz

drive frequency. The computed results are shown in figure 2.4 for each of the modes (*chaotic*, *bullet* and *continuous*).

Initial comparison between the two methods visually demonstrates that both reconstructions delineate the chaotic mode. Indeed the positive current peak deterministic Jitter, as measured in the time-domain, is of the order of $5\mu\text{s}$, which is close to the τ value used in the phase space reconstructions. However, the 3-dimensional phase space reconstructions provide poor visual discrimination between the bullet and continuous modes. This is because the current frequency doubling information contained in the continuous time-domain display is not clearly resolved in the phase space reconstruction. The outcome of this limited comparison suggest that a suitable attractor for representing the three APPJ pen modes can be found within the supposition of n -frames within a current waveform data block. In addition time-domain n -frame suppositions reveal the modes and therefore can be used to characterize and map the time resolved visual properties of each mode, see reference [4].

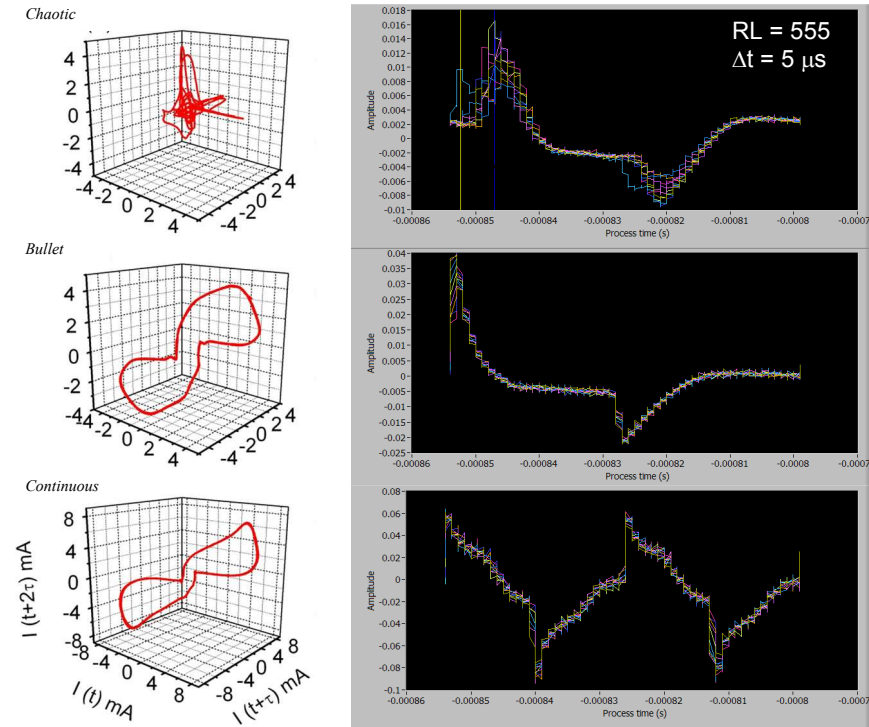


Figure 2.3: APPJ pen phase space reconstruction for each mode.

Figure 2.4: APPJ time-domain n -frame representation for each mode.

3 Deconvolution of a single observation: Electro-acoustic

The PlasmaTreat OpenAir™ APPJ is used worldwide and represents a typical

APPJ in the manufacturing sector. Full technical details of the APPJ are given in references [5, 6]. In this study the APPJ is electrically driven at 19 kHz and the working (ionisation) gas is Air. The first impression of this APPJ that it is much larger than the plasma pencil design, and the sound emitted by this APPJ is generally 30 dB above the environment sound level. This section is concerned with the decoding of the APPJ electro-acoustic emission [10] and the use of parts of the conditioned signal for process control.

As with reference [10] the electro-acoustic signal is captured by a microphone and sampled using a computer soundcard followed by a Fast Fourier Transform. LabVIEW 8.2 software is used to present the raw data in frequency-domain (0-60 kHz span). Within the software a Savitzky-Golay digital filter [11] is chosen to piece-by-piece smooth the raw data by least square minimisation with a polynomial function ($m = 1$) within a moving window. The windowing is express in the following form, where k is the \pm sampled data points.

$$2k + 1$$

Figure 3.1a and b shows the raw un-filtered dataset (gray trace) and the filtered dataset (black trace) under plasma plume free expansion conditions. Experimentally it is found that a $k = 10$ preserves the high Q-factor ($f/\Delta f$ -3 dB bandwidth ~ 200) frequency registration of the 19 kHz drive signal and its harmonics plus reduces the measurement noise floor to -100 dB that results in a signal-to-noise ratio (SRN) of 50 dB ± 3 dB: a 20 dB improvement when compared to the unfiltered dataset SRN. The second feature of note is the 3 broad peaks at 10-11, 25-30 and 45 kHz. The frequency spacing between these peaks may be represented mathematically using a quarter standing-wave closed air-column (clarinet model) [7] and so describes the longitudinal mode within the APPJ nozzle.

$$f_n = \frac{nc}{4(L + 0.6r)}$$

In the above equation, n is modulo frequency number, L is the physical length of the nozzle ($L = 8$ mm), $0.6r$ is the end correction, where r is the internal radius of the nozzle) and c_{sound} is the sound velocity in air. For this model the exit aperture of the nozzle defines the maximum pressure vibration, and the internal nozzle aperture, (where the compressed air is at 1.5 atmospheres) is the antinode. Using this quarter standing-wave model only the fundamental and odd number overtones are supported. For example, f_0 and $n = 3, 5, \text{etc.}$. This model, at room temperature 25°C (where the speed of sound in air equates to 346.26 m.s⁻¹) yields frequency values of $f_n = 9.11$ kHz, $f_3 = 27.33$ kHz, and $f_5 = 45.55$ kHz. The values of f_n and $f_3 = 3$ approximates to the broad peaks observed in figure 3.1a.

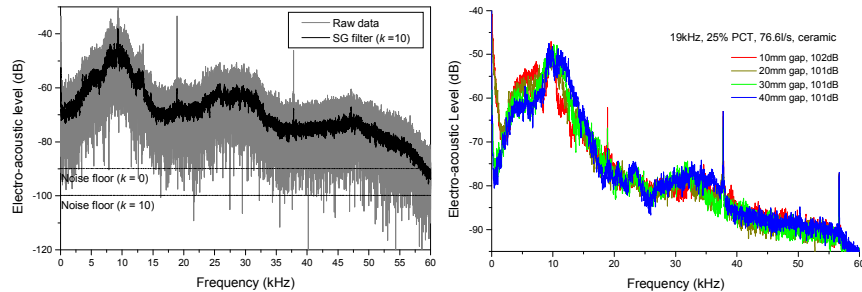


Figure 3.1a: APPJ raw signal and SG filtered signal. Figure 3.1b: APPJ SG filtered signal as a function nozzle-surface distance.

Having established the typical spectrum of the APPJ electro-acoustic emission, the focus of this section now moves to examining the electro-acoustic signal as a function APPJ nozzle to surface distance, or gap. Figure 3.1.b provides four measurements at gaps: 10, 20, 30 and 40 mm at $k = 10$. Under these conditions the electrical drive at $f_0 = 19$ kHz and its harmonics ($f_2 = 38$ kHz and $f_3 = 57$ kHz) are constant in their frequency registration. In addition the three broad peaks are still present. However a new broad peak at 4-8 kHz emerges and grows in amplitude as the gap distance is reduced. In addition, sound pressure level measurements indicate an increase of 1 dB from 101 to 102 dB.

The information obtained from this study allows the single observable electro-acoustic signal to be tested for specific conditions at discrete frequency bands. This procedure is readily implemented in LabVIEW software using lower and upper limits at the discrete frequency bands. When the signal amplitude breaches these limits, an out of bound condition fail is registered and a simple audio-visual alarm is triggered to warn the operator, or a binary code (0 or 1) from the comparator [30] may also be hard wired for data logging.

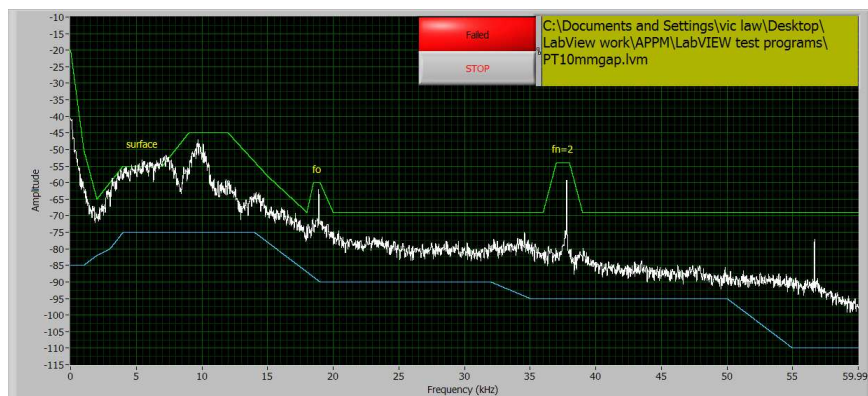


Figure 3.2: A LabVIEW screen data demonstrating how the system can be used for process control. In this case 'Fail' is associated with variation in signal in the 4 to 8 kHz frequency range.

The ability to locate a surface has many technological uses including 3-

dimensional imaging of plasma treated topographical surfaces. This section presents a LabVIEW program [10] that records the electro-acoustic emission, as the APPJ traverse back and forth across a metal work piece, and transfers the sequentially sampled data points into n-frames within a block to produce a 3-D image of the topographical surface. Figure 3.3 provides a simplified block diagram of the software where some of the control subroutines (vi(s)) have been removed for clarity.

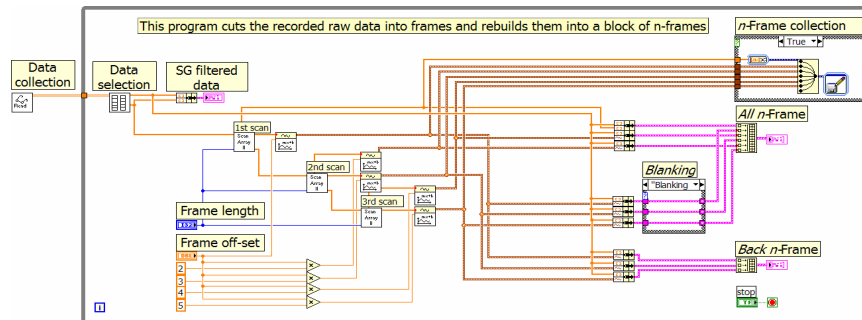


Figure 3.3: Simplified block diagram of the 3-D surface imaging software.

Figure 3.4 provides a 3-dimensional image of a 10 mm wide by 2 mm thick plate with a 2 mm diameter hole drilled in the middle of the surface. Each of the 9 scans is off-set by 2 mm, with the first scan recording the CNC positioning the APPJ to the start of the plasma process. Only the forward scans are recorded with the return blanked off. Note the acoustic discontinuity where the 2 mm hole is located.

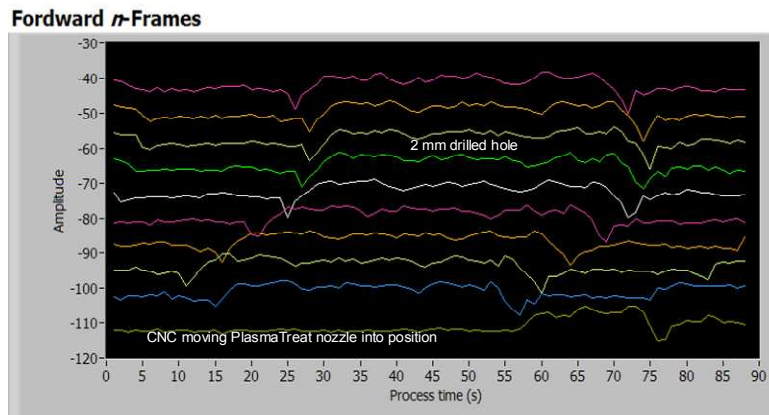


Figure 3.4: Nine scan 3-D surface image of metal surface with a 2 mm hole. Blanking turned on.

4 Conclusions

Atmospheric pressure plasma jets offer enhanced quality of care at reduced cost

and will be of immense societal and commercial value. This invited paper has reviewed both time-domain current waveforms and deconvolution of electro-acoustic emission (in the frequency-domain) of two (hand-held and industrial scale APPJ systems). In the first case, 3-dimensional delay embedding was compared to periodic analysis using n -frames within a data block was compared. Both techniques provide information on the chaotic mode, with the latter yielding information on all three modes.

For the industrial scale system, single scalar time series, in the form of electro-acoustic emission is readily available. Here temporal-spatial deconvolution of the data provides information on the jet nozzle surface location and surface topology.

Acknowledgements

This work is supported by Science foundation Ireland 08/SRC/I1411. MGK, FI and JLW thank support from EPSRC.

References

1. M. G. Kong, G. Kroesen, G. Morfill, T. Nosenko, T. Shimizu, J. van Dijk and J. L. Zimmermann. Plasma medicine: an introductory review. *New Journal of Physics*, Vol. 9, 115012 (35pp), 2009.
2. R. Suchentrunk, H. J. Fuessler, G. Staudigl, D. Jonke, and M. Meyer. Plasma surface engineering - innovative processes and coating systems for high-quality products. *Surface and Coatings Technology*, vol. 112, no. 1-3, 351-357, 1999.
3. J. Ringwood, S. Lynn, G. Bacilli, B. Ma, E. Ragnoli and S. Mcloone. Estimation and Control in Semiconductor etch: practice and possibilities. *IEEE, Trans, Semicond, Manuf*, vol. 23, no.1, 87-96, 2010.
4. J. L. Walsh, F. Iza, N. B. Janson, V. J. Law and M. G. Kong Three distinct modes in a cold atmospheric pressure plasma jet. *J, Phys, D: Appl, Phys*, vol. 43, no. 7, 075201 (14pp), 2010.
5. D. P. Dowling, F. T. O'Neill, S. J. Langlais and V. J. Law, Influence of dc pulsed atmospheric pressure plasma jet processing conditions on polymer activation. *Plasma Process Polym*. Vol 8 no. 6, 2010. DOI: 10.1002/ppap.201000145.
6. V. J. Law, F. T. O'Neill and D. P. Dowling. Evaluation of the sensitivity of electro-acoustic measurements for process monitoring and control of an atmospheric pressure plasma jet system. *PSST*. Vol. 20, no. 3, 035024, 2011.
7. N. Packard, J. Crutchfield, D. Farmer, and R. Shaw. Geometry from time series. *Phys. Rev. Lett*, vol. 45, no. 9, 712-716, 1990.
8. A M Fraser and H L Swinney. Independent coordinates for strange attractors from mutual information. *Phys. Rev A*, vol. 33, no. 2, 1134-1140, 1986.
9. The LabVIEW software can be obtained from the principal author: vic.law@dcu.ie
10. V J Law, C E Nwankire, D P Dowling, and S Daniels. Acoustic emission within an atmospheric helium corona discharge jet. "*Chaos Theory: Modeling, Simulation and Applications*." Editors: C H. Skiadas, I Dimotikalis and C Skiadas. Publisher: World Scientific Publishing Co Pte Ltd. pp 255-264, 2011.
11. A. Savitzky, and M. J. Golay. Smoothing and differentiation of data by simplified least squared procedures. *Analytical chemistr*, vol. 36, no.8, 1627-2639, 1964.